The Planetary Science Journal, 1:9 (6pp), 2020 June https://doi.org/10.3847/PSJ/ab8638

Physical Properties of 299 NEOs Manually Recovered in Over Five Years of NEOWISE Survey Data

Joseph R. Masiero[1], Patrice Smith[1,2], Lean D. Teodoro[1,3], A. K. Mainzer[4], R. M. Cutri[5], T. Grav[4], and E. L. Wright[6]
[1] Jet Propulsion Laboratory/California Institute of Technology, 4800 Oak Grove Dr., MS 183-301, Pasadena, CA 91109, USA; Joseph.Masiero@jpl.nasa.gov
[2] University of Hawaii, Hilo, HI 96720, USA
[3] University of Hawaii, Manoa, HI 96822, USA
[4] University of Arizona, Tucson, AZ 85721, USA
[5] California Institute of Technology, IPAC, 1200 California Blvd., Pasadena, CA 91125, USA
[6] University of California, Los Angeles, CA 90095, USA
Received 2020 February 26; revised 2020 March 31; accepted 2020 April 1; published 2020 April 22

Abstract

Thermal infrared measurements of near-Earth objects (NEOs) provide critical data for constraining their physical properties such as size. The Near-Earth Object Wide-field Infrared Survey Explorer (NEOWISE) mission has been conducting an all-sky infrared survey to gather such data and to improve our understanding of this population. While automated routines are employed to identify the majority of moving objects detected by NEOWISE, a subset of objects will have dynamical properties that fall outside the window detectable to these routines. Using the population of known NEOs, we have conducted a manual search for detections of these objects that were previously unreported. We report 303 new epochs of observations for 299 unique NEOs of which 239 have no previous physical property characterization from the NEOWISE Reactivation mission. As these objects are drawn from a list with inherent optical selection biases, the distribution of measured albedos is skewed to higher values than is seen for the diameter-selected population detected by the automated routines. These results demonstrate the importance and benefit of periodic searches of the archival NEOWISE data.

Unified Astronomy Thesaurus concepts: Asteroids (72); Near-Earth objects (1092); Infrared astronomy (786); Infrared photometry (792)

Supporting material: machine-readable table

1. Introduction

Small bodies of the solar system with perihelia less than 1.3 au are known as near-Earth objects (NEOs). These objects are warmed by incident sunlight, and re-emit that light as thermal infrared emission, with objects that are closer to the Sun being warmer and thus brighter at infrared wavelengths. The Near-Earth Object Wide-field Infrared Survey Explorer (NEOWISE) has been carrying out a survey of the sky at thermal infrared wavelengths to detect and characterize these NEOs (Mainzer et al. 2014a). NEOWISE began its survey on 2013 December 13 after the reactivation of the Wide-field Infrared Survey Explorer spacecraft (WISE; Wright et al. 2010; Mainzer et al. 2011a) and has continued surveying for over 6 yr at 3.4 and 4.6 μm (referred to as W1 and W2, respectively). The images obtained by NEOWISE are automatically scanned for detections of moving solar system objects, and these detections are reported regularly to the Minor Planet Center (MPC) as part of regular survey data processing. Thermal modeling can be performed on these detections allowing for diameters to be constrained, as well as albedos when visible light measurements are also available, and these parameters for objects observed during the NEOWISE Reactivation mission have been described in a series of papers (Mainzer et al. 2014a; Nugent et al. 2015, 2016; Masiero et al. 2017, 2020).

The automated WISE Moving Object Processing System (WMOPS) searches the NEOWISE data within a set of bounds that allow it to detect most, but not all, NEOs passing through the field of view. Tracklets are built from chains of detections, within set limits on acceleration, changing direction of motion, and a minimum number of observations. These limits are set to maximize the number of objects identified while maintaining a reasonable number of false-positives sent for human quality assurance (see Cutri et al. 2015). These limits will, however, mean that some objects of interest will not be identified. Specifically, NEOs passing close to NEOWISE, and thus having a high rate of motion through the field of view, are less likely to meet the threshold of the minimum of five detections to be identified automatically. Other objects, based on viewing geometry, will exceed the allowable changes in the rate and direction of motion for linking.

Because NEOWISE archives all full-frame images acquired during the survey and a database of sources detected in those images, it is possible to conduct a search for known NEOs missed by the automated processing after the fact. We present in this work a search for these objects, using the list of all currently known NEOs as of 2019 June 1 as an input. A previous search to this effect was performed by Masiero et al. (2018), covering the first three years of the NEOWISE Reactivated survey, while Mainzer et al. (2014b) presented a similar search of the data from the cryogenic portion of the original WISE survey. This work uses the larger list of NEOs known presently, as well as all data from the first five and a half years of the NEOWISE Reactivation data. The aim of this search is to increase the number of NEOs with diameter and albedo characterization in order to expand our knowledge of this population and to make best use of the data obtained by the NEOWISE mission.

2. Methods

For our search, we used the list of all known NEOs recorded in the MPC's orbital element list MPCORB[7] as of 2019 June 1. Using these orbital elements, we determined the subset of objects that were at Solar elongations between 88° and 115° (the NEOWISE field of regard during the mission) and predicted apparent magnitudes of $V < 20$ mag during the time of the NEOWISE Reactivation survey. Each object on this list was queried from one month before to one month after the date of peak brightness in the searched elongation region using the IRSA (Infrared Science Archive) WISE Moving Object Search Tool[8] through the API. These searches produced a list of WISE images that overlapped the predicted position of each NEO and thus might contain a previously unidentified detection.

The images were visually inspected to look for sources coincident with the predicted positions of each object. Images without identifiable sources were removed from the list, and then the NEOWISE-R Single Exposure Source Table[9] was searched for entries within 5″ of the predicted position of each NEO at the time of the NEOWISE observation. Objects with NEOWISE observations already reported to the MPC by the automated WMOPS system were not included in this search for the epochs that had been reported. However, this search did return additional detections for previously reported NEOs at new epochs. Increasing the number of identified observing epochs for NEOs is critical for advanced thermophysical modeling work that uses multiple viewing geometries to constrain NEO surface thermal inertias (e.g., Delbo et al. 2007, 2015; Koren et al. 2015; Hanus et al. 2016; Masiero et al. 2019, etc.).

The resulting list of returned detections contained objects with as few as one detection to as many as 34 detections. For objects detected in only a single image, there is a significant potential for stars, cosmic rays, or other artifacts and noise sources to masquerade as real detections, so a second visual inspection of these detections was carried out. After this inspection, 48 NEOs with single detections were determined to have a high probability of being real, and 38 of these were detected in both NEOWISE bandpasses (which are imaged simultaneously).

Objects detected five or more times are of particular interest because they represent tracklets that could have been identified by the WMOPS automated processing routines but were not for various reasons. The WMOPS software identifies objects by first creating pairs of detections and then linking these pairs based on common motion vectors. The WMOPS velocity limits on creating pairs ($0.021\,\mathrm{deg\ day^{-1}} < \mathrm{velocity} < 3.22\,\mathrm{deg\ day^{-1}}$) along with the acceleration tolerance ($<0.01\,\mathrm{deg\ day^{-2}}$) and the angle of motion tolerance ($<1°$) used for linking them define a phase space where WMOPS can detect objects. The majority of the NEOs with five or more detections found in our manual search here are outside this phase space, as shown in Figure 1. The remaining 21 objects that are within this phase space were lost either because they were near the signal-to-noise ratio detection limit ($S/N > 4.5$) used to compile the input list to build detection pairs, or they were in a region of sky with a dense background and so were lost during the catalog-based filtering for stationary object rejection that is done at the beginning of WMOPS processing.

[7] https://www.minorplanetcenter.net
[8] https://irsa.ipac.caltech.edu/applications/MOST/
[9] https://irsa.ipac.caltech.edu/

It is important to note that the vast majority of NEOs were discovered by ground-based visible light telescopes and thus will have a preferential bias toward high-albedo objects at any given size range, as visible surveys are brightness-limited. This bias will combine with the selection bias we impart by looking for objects with visually bright apparitions at the time they approached the NEOWISE field of regard, resulting in our list preferentially containing more high-albedo asteroids than would be found in an unbiased sample of the true NEO population.

3. Thermal Modeling

We employed the Near-Earth Asteroid Thermal Model (NEATM; Harris 1998) to constrain the physical properties of the detected asteroids using their NEOWISE thermal infrared measurements, following the procedure used in our previous study of NEOWISE manually recovered NEOs (Masiero et al. 2018). Using the tables of detections published in IRSA, we extract the W1 and W2 profile-fit photometry and astrometry for the detections of these objects. In addition to visual inspection of all detections to remove contamination from cosmic rays, artifacts, and background stars, we also performed an automated filtering on the detections before using them for thermal modeling, as described below.

Every detection published in IRSA includes a reduced χ^2 (*rchi*2) value of the fit of the point-spread function (PSF) model to the presumed source in each bandpass. We reject all detections with $rchi2 > 20$, as this indicates a high likelihood of a contaminated detection. In general, values of $rchi2 > 5$ are removed from the analysis as they have a higher likelihood of being cosmic rays (e.g., Masiero et al. 2020). However, any source that is trailed, even at the sub-PSF level, may have an increased *rchi*2 value, and so for this work, we only reject sources with $rchi2 > 20$ to remove the most serious cosmic ray contamination. This cut was determined through visual validation of the detections of singleton objects that were slightly trailed and seen in both bands, providing a guide for what the largest acceptable *rchi*2 would be for this work.

We also reject two-band detections where W1–W2 < 1 mag to remove contamination from stars. During initial thermal modeling tests, we found instances of detections contaminated by comparably bright stars, which created problems for the thermal model fitting. The majority of stars are in the Rayleigh–Jeans portion of their spectral energy distribution at the W1 and W2 wavelengths, so the expected W1–W2 color is ~0, while for sources with rising thermal emission in W2, such as asteroids inside ~3 au, this color is expected to be redder. An analysis of the W1–W2 colors of all sources detected in two bands shows a peak of the distribution at W1–W2 ~ 2.6 mag, with the vast majority of sources within 1.5 mag of that peak. Visual inspection of sources with W1–W2 < 1 mag confirmed the predicted positions coincide with stationary background objects, so this color is used as a cut on the data prior to thermal modeling. In total, 40 detections (out of 1688) were eliminated from fitting by color and *rchi*2 cuts. This cut would also reject distant asteroids dominated by reflected light in the W1 and W2 bands; however, these are highly unlikely to have large rates of motion and be missed by WMOPS, if bright enough to be detected.

Proximity of the asteroid to the WISE spacecraft is the main reason that objects will be moving too fast or accelerating too much to be detected often enough for automated identification.

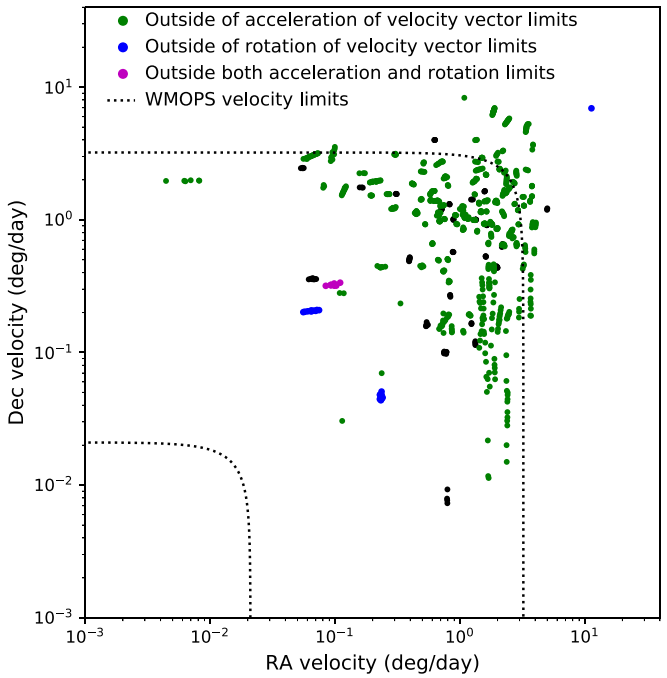

Figure 1. Rates of motion in R.A. and decl. of all objects presented here that were detected more than five times (the minimum required for automated detection). Each tracklet will be shown as a string of dots based on the changes in motion within the tracklet. Dotted lines show the lower and upper limits to the rate of motion that WMOPS will detect. Green points are tracklets that had accelerations beyond the limit accepted by WMOPS. Blue points had rotations in the angle of motion outside the WMOPS limit. Purple points are tracklets the exceeded both limits. Black points within the WMOPS velocity limits were not found either due to them falling below the detection threshold or having detections rejected by the atlas-based stationary object rejection routines.

As NEOWISE observes at a narrow range of Solar elongations, the observer distance and observational phase angle are coupled. This results in the detections presented here being made at higher phase angles than NEOs discussed in previous work (Nugent et al. 2015, 2016; Masiero et al. 2017). The NEATM beaming parameter, used to account for model uncertainties, is correlated with phase (Mainzer et al. 2011b), and as such we assume a larger beaming parameter here than is used for other studies of NEOWISE-observed NEOs. Following Masiero et al. (2018), we assume model beaming parameters of $\eta = 2.0 \pm 0.5$. We also assume ratios of the infrared albedo at 3.4 μm ($p_{\rm IR}$) to the visual albedo of $p_{\rm IR}/p_V = 1.6 \pm 1.0$. The uncertainties on these parameters are fed into our Monte Carlo analysis to determine overall diameter uncertainty.

We employ a Monte Carlo analysis of our fit to constrain the statistical uncertainty on our diameter determinations. Taking the uncertainties on our measured parameters as well as the assumed uncertainty on our fixed model parameters as discussed above, we vary each input to our model over 25 iterations and use the resultant spread of the diameters and albedos in the model solutions as the quoted uncertainty on our best-fit values. For the W1 and W2 magnitudes, measurement uncertainties are taken from the Single Exposure Source Table. For the measured H magnitude, we assume an uncertainty of 0.2 magnitudes following previous work (e.g., Masiero et al. 2018), as no uncertainty is provided in the MPC catalog. We assume all parameters can be modeled by a Gaussian distribution, with the uncertainties giving the 1σ value and the measured/assumed value as the mean of the distribution. We note that for the flux uncertainties specifically, Wright et al. (2018) showed that while they are not strictly Gaussian, the actual measurement uncertainty can be encompassed by a Gaussian using the published value. Thus, this assumption is sufficient for our analysis where the fit uncertainties are dominated by other terms, such as the unknown beaming parameter.

In addition to statistical uncertainties on the thermal model fits, there are also systematic model uncertainties to consider. NEATM is an imperfect model that assumes the night side of an asteroid contributes no thermal emission. While this will only have a small effect on objects at low phase angles, at higher phases, this results in an underestimation of the emitted flux and an overestimation of the diameter. Mommert et al. (2018) showed that beyond a phase angle of $\alpha > 65°$, NEATM deviates from the true diameter and requires a correction factor to accurately reproduce input thermophysical model parameters. The objects in our sample have a mean phase angle of $\alpha = 73°$, and three-quarters of them were seen at phases beyond $\alpha = 65°$. In light of this, we also calculated the corrected diameters and albedos based on the correction equations from Mommert et al. (2018). However, we note that this correction was developed from a NEATM model fit to multiple wavelengths spanning the peak of thermal emission and so may not completely correct for the model offsets in our implementation of NEATM.

A further source of uncertainty for the fits presented in this work is the unknown light-curve phase for objects with a small number of detections. As discussed in Mainzer et al. (2014b) and Masiero et al. (2018), when an object has only a few samplings of its light curve available, the error on determining the mean of the light curve (which enables fitting an effective spherical diameter for a body) increases, up to ~30% of the light-curve amplitude for a single detection. For an object with a light-curve amplitude of >1 mag, this can result in an offset of the fitted diameter from the true spherical equivalent diameter of >15%. In addition to this effect, light-curve variations as well as the Eddington bias can result in objects near the detection limit having overestimated fluxes, artificially increasing the fitted diameter compared to the true size. For the objects presented here, our median S/N in W2 was larger than 10, so this will not have a significant impact on these fits but should be kept in mind when dealing with objects with a small number of detections.

4. Results and Discussion

The results of our modeling, including the best-fit values and Monte Carlo error analyses, are presented in Table 1. We describe 303 NEATM fits of 299 unique NEOs, of which 239 had not been previously characterized by the Reactivated NEOWISE mission. The remaining 60 objects had been detected and reported by the spacecraft at a different observing epoch since the reactivation in 2013 December. The four objects with multiple fits show good agreement within the quoted statistical uncertainties from the Monte Carlo analysis. For all objects and epochs, the measured astrometry data have been reported to the MPC and are archived there.

Previous work has shown that fits of objects with reflected light contributions to the W2 band above 10% of the total flux are less reliable (see Masiero et al. 2017), and thus we removed 19 objects from our physical property list fits that were detected by NEOWISE but fell in this regime. These objects were: (152952), (163132), (163243), (281375), (304640), (364136),

Table 1
Thermal Model Fits for Manually Recovered NEOs Detected in the NEOWISE Reactivation Survey Data

Name	Input H (mag)	G	Diameter (km)	$D_{\rm corr}$ (km)	p_V [a]	$p_{V\,\rm corr}$	Beaming	$n_{\rm W1}$	$n_{\rm W2}$	Phase (deg)	Mean MJD days
85275	16.10	0.15	3.614 ± 1.475	3.643	0.049 (+0.123/−0.035)	0.048	2.00 ± 0.50	0	1	37.11	57329.3314
85713	15.60	0.15	3.442 ± 1.028	3.098	0.108 (+0.074/−0.044)	0.134	2.00 ± 0.50	5	5	75.50	56977.7030
85953	18.10	0.15	0.959 ± 0.207	0.922	0.122 (+0.058/−0.039)	0.134	2.00 ± 0.50	3	3	63.29	58220.0983
85989	17.10	0.15	2.986 ± 1.041	2.978	0.052 (+0.043/−0.023)	0.053	2.00 ± 0.50	13	13	49.39	56875.8718
85990	20.20	0.15	0.404 ± 0.108	0.342	0.113 (+0.069/−0.043)	0.153	2.00 ± 0.50	2	2	83.11	57023.2583
86819	17.40	0.15	1.124 ± 0.259	1.043	0.259 (+0.165/−0.101)	0.304	2.00 ± 0.50	16	17	70.67	56934.4738
88213	19.40	0.15	0.940 ± 0.249	0.893	0.050 (+0.030/−0.019)	0.056	2.00 ± 0.50	6	6	66.03	58195.2370
89959	16.40	0.15	1.903 ± 0.617	1.893	0.162 (+0.138/−0.075)	0.167	2.00 ± 0.50	6	6	50.85	58374.7789
90416	18.60	0.15	2.001 ± 0.703	1.797	0.041 (+0.034/−0.018)	0.050	2.00 ± 0.50	3	3	75.85	57071.5748
96590	16.20	0.15	1.737 ± 0.446	1.583	0.159 (+0.092/−0.058)	0.192	2.00 ± 0.50	4	4	73.58	58167.5872

Notes. Names are in MPC-packed format, H and G are the input photometric parameter measurements used by the model, p_V is the visible light albedo, and $n_{\rm W1}$ and $n_{\rm W2}$ are the numbers of detections in the W1 and W2 bandpasses. $D_{\rm corr}$ and $p_{V\,\rm corr}$ have been corrected following the equations in Mommert et al. (2018).
[a] Albedo uncertainties are symmetric in log-space as the error is dominated by the uncertainty on H; the asymmetric linear equivalents of the 1σ log-space uncertainties are presented here.

(This table is available in its entirety in machine-readable form.)

(388945), (418198), (472263), (530743), (536531), 2009 FU23, 2017 OO1, 2017 RV17, 2017 VX1, 2017 VW13, 2018 RP8, 2018 UY, and 2019 CE. The astrometry for these objects recovered in our search were still submitted to the MPC.

We show in Figure 2 a comparison of the diameters and albedos for the objects presented here, along with those published from our previous manual recovery search (Masiero et al. 2018) and the fits for objects found by our automated WMOPS detection algorithms. As expected, the bias in favor of high-albedo objects (due to the initial discovery selection effect combined with the selection effect on the input list for our search) is clearly apparent in the distribution of our sample, with the majority of objects having fits in the with albedos greater than $p_V > 0.1$. This work recovered more large objects than our previous manual search, with 78 objects having fitted diameters larger than 1 km. This is because our new search included all objects in the NEO orbital list, while our previous work focused on short-arc asteroids that had been discovered more recently. More recently discovered objects tend to be smaller as there are fewer large objects that remain undiscovered as the global NEO survey programs progress.

We can use the 60 objects that have previously reported NEOWISE Reactivation diameters to verify the accuracy of the model results presented here. We show in Figure 3 the comparison of the diameters presented in this paper to those previously published values. The diameters in this work show a fairly large random scatter, as well as a systematic offset to larger values. This is likely due to a combination of effects, including the smaller number of detections that present a bias toward light-curve maxima, as well as the larger phase angles of observation that are detrimental to the NEATM fitting accuracy. Although we include the correction to the NEATM fits proposed by Mommert et al. (2018), which provides a small improvement to this offset, it does not fully eliminate it.

We can also compare our physical property results to those NEOs with sizes measured by the Spitzer space telescope (Trilling et al. 2016). The objects targeted by Spitzer are generally are smaller than those regularly detected by the NEOWISE automated pipeline, but our manual recovery allows us to find more objects in this smaller size range. We extracted all NEOs with Spitzer CH2 S/N > 5 from the online database of

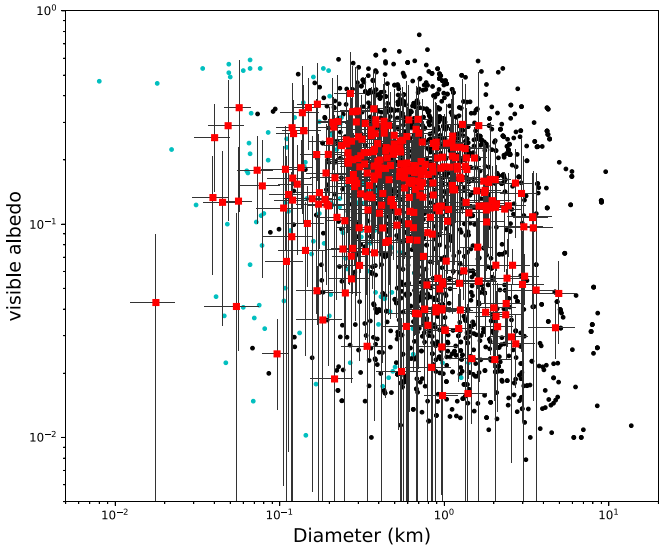

Figure 2. Diameters and albedos for NEOs presented here (red squares), compared with manually detected NEOs presented in Masiero et al. (2018; cyan dots) and NEOs detected automatically in the first five years of the NEOWISE Reactivation survey (black dots). Error bars are shown only for the newly presented objects but are comparable in size for all fits. The search criteria used here that targets objects with predicted visual magnitudes brighter than $V = 20$ mag at the time they passed through the NEOWISE field of regard, combined with the preferential discovery of high-albedo objects by optical telescopes, results in a significant bias against low albedo NEOs.

fitted properties.[10] There are 105 objects from there in common with our table of fitted properties. A comparison between the sizes published in these two data sets is shown in Figure 4.

The fits presented here here tend to be somewhat larger than those derived from the Spitzer data, though not as large as the offset from previous NEOWISE epochs. Due to the limited time window over which Spitzer observed most NEOs, those data may show some of the same effects and biases associated with limited light-curve sampling as our fits; however, this effect will be more pronounced for objects seen by NEOWISE in a small number of short exposures. Additionally, the larger beaming

[10] http://neareathobjects.nau.edu

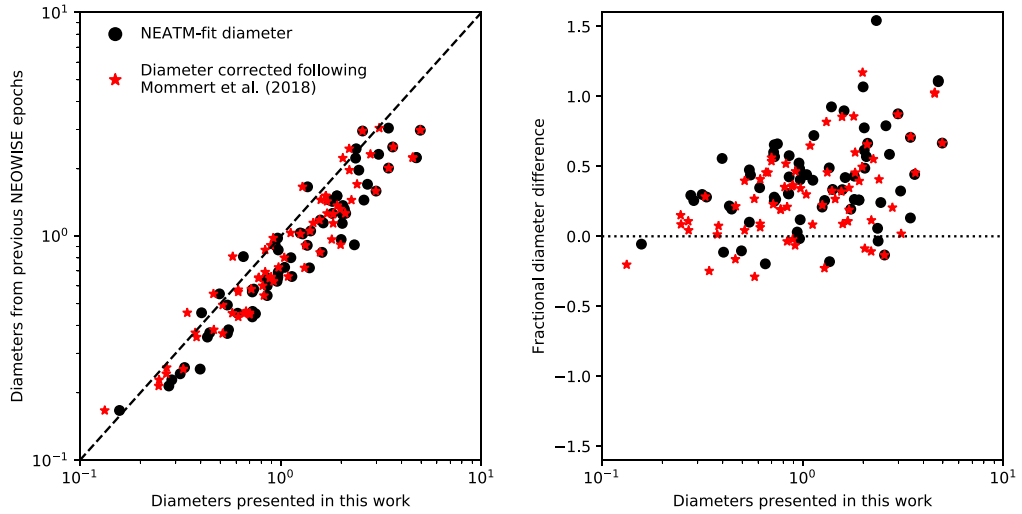

Figure 3. Comparison of the diameters presented in this work to previously published NEOWISE diameters of the same NEOs at different observing epochs (left). Fits from the NEATM model are shown as black circles, and sizes corrected following (Mommert et al. 2018) are shown as red stars. The fractional difference between these fits (right) shows that the NEATM fits to the higher phase angle data tends to overestimate the sizes compared to previous work.

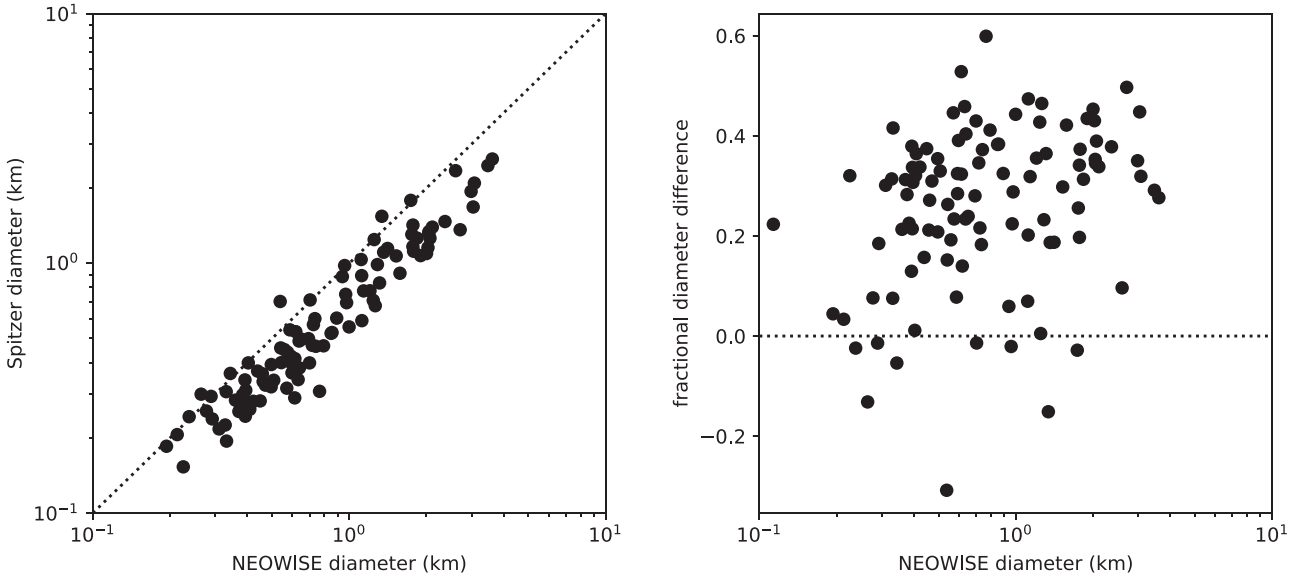

Figure 4. Comparison of NEO diameters presented here to sizes determined by Spitzer (left) and fractional diameter difference between the two data sets (right). Sizes derived here are larger than those found by Spitzer by ∼30%, which is a result of the larger assumed beaming parameter chosen here.

parameter used for our fits (due to the typically higher phase angle of observation) also will skew the fits to a larger size.

Given the results of these comparisons, the diameters presented here may be overestimates of the actual spherical equivalent diameter. This highlights the limitations of NEATM as well as the need to use thermophysical models for objects with high phase angle observations to more accurately constrain sizes. Performing thermophysical modeling on the NEOWISE and Spitzer observations together would further enhance the benefits of this technique.

5. Conclusions

We present diameter fits for 299 NEOs found through manual searches of the NEOWISE data archive, 239 of which had no previously reported NEOWISE-derived diameter. Due to the detection circumstances of these objects, and the larger phase angles at which they are observed compared to the automatically detected objects, the uncertainty on the diameter determination is larger, and there is a systematic offset in the fitted diameters to larger sizes in this work. Thus, the diameters presented in many cases represent overestimates of the true effective spherical diameter of these bodies. These observations, however, do provide some constraint on the overall size of these NEOs and are important additions to the multiple observing epochs needed to carry out more advanced thermophysical modeling.

When combined with all previous publications, the diameters presented here bring the total number of NEOs characterized by the NEOWISE Reactivation mission to 1193 since the survey was restarted in 2013 December. Combined with objects observed during the initial WISE mission phases before hibernation, a total of 1652 NEOs have physical property characterizations using data from the WISE and NEOWISE missions. As NEOs continue to be discovered by ongoing and future surveys, the archived NEOWISE single-frame images will be an important resource for recovering characterization data well after the mission has ended. The

NEOWISE data are already an important legacy data set with a large amount of information not currently known that is waiting to be revealed.

The research was carried out at the Jet Propulsion Laboratory, California Institute of Technology, under a contract with the National Aeronautics and Space Administration (80NM0018D004). This publication makes use of data products from the Wide-field Infrared Survey Explorer, which is a joint project of the University of California, Los Angeles, and the Jet Propulsion Laboratory/California Institute of Technology, funded by the National Aeronautics and Space Administration. This publication also makes use of data products from NEOWISE, which is a joint project of the University of Arizona and Jet Propulsion Laboratory/California Institute of Technology, funded by the Planetary Science Division of the National Aeronautics and Space Administration. This research has made use of data and services provided by the International Astronomical Union's Minor Planet Center. This research has made use of the NASA/IPAC Infrared Science Archive, which is operated by the California Institute of Technology, under contract with the National Aeronautics and Space Administration. This research has made extensive use of the *numpy*, *scipy* (Virtanen et al. 2020), *astropy* (Astropy Collaboration et al. 2013, 2018), and *matplotlib* Python packages.

ORCID iDs

Joseph R. Masiero https://orcid.org/0000-0003-2638-720X
R. M. Cutri https://orcid.org/0000-0002-0077-2305
T. Grav https://orcid.org/0000-0002-3379-0534
E. L. Wright https://orcid.org/0000-0001-5058-1593

References

Astropy Collaboration, Price-Whelan, A. M., Sipőcz, B. M., et al. 2018, AJ, 156, 123
Astropy Collaboration, Robitaille, T. P., Tollerud, E. J., et al. 2013, A&A, 558, A33
Cutri, R. M., Mainzer, A., Conrow, T., Masci, F., Bauer, J., et al. 2015, Explanatory Supplement to the NEOWISE Data Release Products (Pasadena, CA: CalTech) http://wise2.ipac.caltech.edu/docs/release/neowise/expsup/
Delbo, M., Mueller, M., Emery, J. P., Rozitis, B., & Capria, M. T. 2015, in Asteroids IV, ed. P. Michel, F. DeMeo, & W. F. Bottke (Tucson, AZ: Univ. Arizona Press), 107
Delbo, M., dell'Oro, A., Harris, A. W., Mottola, S., & Mueller, M. 2007, Icar, 190, 236
Hanuš, J., Delbo', M., & Vokrouhlický, D. 2016, A&A, 592, 34
Harris, A. W. 1998, Icar, 131, 291
Koren, S. C., Wright, E. L., & Mainzer, A. K. 2015, Icar, 258, 82
Mainzer, A. K., Bauer, J., Cutri, R., Grav, T., Masiero, J., et al. 2014a, ApJ, 792, 30
Mainzer, A. K., Bauer, J., Grav, T., Masiero, J., Cutri, R., et al. 2014b, ApJ, 784, 110
Mainzer, A. K., Bauer, J. M., Grav, T., Masiero, J., et al. 2011a, ApJ, 731, 53
Mainzer, A. K., Grav, T., Bauer, J. M., Masiero, J., et al. 2011b, ApJ, 743, 156
Masiero, J. R., Mainzer, A. K., Grav, T., et al. 2020, PSJ, 1, 5
Masiero, J. R., Nugent, C., Mainzer, A. K., Wright, E., Bauer, J., et al. 2017, AJ, 154, 168
Masiero, J. R., Redwing, E., Mainzer, A. K., Bauer, J. M., Cutri, R. M., et al. 2018, AJ, 156, 60
Masiero, J. R., Wright, E. L., & Mainzer, A. K. 2019, AJ, 158, 97
Mommert, M., Jedicke, R., & Trilling, D. 2018, AJ, 155, 74
Nugent, C. R., Mainzer, A., Bauer, J. M., Cutri, R. M., Kramer, E., et al. 2016, AJ, 152, 63
Nugent, C. R., Mainzer, A., Masiero, J., Bauer, J. M., Cutri, R. M., et al. 2015, ApJ, 814, 117
Trilling, D. E., Mommert, M., Hora, J., et al. 2016, AJ, 152, 172
Virtanen, P., Gommers, R., Oliphant, T., et al. 2020, Nat. Methods, 17, 261
Wright, E. L., Eisenhardt, P., Mainzer, A. K., Ressler, M. E., Cutri, R. M., et al. 2010, AJ, 140, 1868
Wright, E. L., Mainzer, A. K., Masiero, J., et al. 2018, arXiv:1811.01454